PCCP

Accepted Manuscript

ROYAL SOCIETY OF CHEMISTRY

www.rsc.org/pccp

Physical Chemistry Chemical Physics
CREATED USING THE RSC LaTeX PCCP ARTICLE TEMPLATE – SEE www.rsc.org/electronicfiles FOR DETAILS
ARTICLE TYPE
www. rsc.org/xxxxxx | XXXXXXXX

From Charge-Transfer to Charge-Separated State: A Perspective from the Real-Time TDDFT Excitonic Dynamics

Alessio Petrone,[a,b] David B. Lingerfelt,[a] Nadia Rega,[b,c] and Xiaosong Li[a*]

Received Xth XXXXXXXXXX 20XX, Accepted Xth XXXXXXXXX 20XX
First published on the web Xth XXXXXXXXXX 200X
DOI: 10.1039/b000000x

'In-Chain Donor/Acceptor block copolymers' comprised of alternating electron rich/poor moieties are emerging as promising semiconducting chromophores for use in organic photovoltaic devices. The mobilities of charge carriers in these materials are experimentally probed using gated organic field-effect transistors to quantify electron and hole mobilities, but a mechanistic understanding of the relevant charge diffusion pathways is lacking. To elucidate the mechanisms of electron and hole transport following excitation to optically accessible low-lying valence states, we utilize mean-field quantum electronic dynamics in the TDDFT formalism to explicitly track the evolution of these photo-accessible states. From the orbital pathway traversed in the dynamics, *p* and *n* type conductivity can be distinguished. The electronic dynamics for the studied polymers show the time-resolved transitions between the initial photoexcited state, a tightly-bound excitonic state that is dark to the ground state, and a partially charge separated state indicated by long-lived, out-of-phase charge oscillations along the polymer backbone. The frequency of these charge oscillations yields insight into the characteristic mobilities of charge carriers in these materials. When the barycenters of the electron and hole densities are followed during the dynamics, a pseudo-classical picture for the translation of charge carrier densities along the polymer backbone emerges that clarifies a crucial aspect in the design of efficient organic photovoltaic materials.

1 Introduction

Bulk heterojunction (BHJ) polymer solar cells, in which conjugated 'electron donor' polymers are blended with 'acceptor' materials (typically fullerene derivatives) represent one promising route to realizing the goal of low-cost and scalable renewable energy [1,2]. While organic BHJ devices currently fall well short of their inorganic counterparts with regard to performance, power conversion efficiencies (PCE) are continually improving with respectable PCEs of 8-9 % now attainable in small, single junction cells.[3,4]

One of the most important advances in the rational design of BHJ devices has been the development of narrow band gap donor polymers that are tuned to better match the solar spectrum.[5,6] Many of these next-generation polymers are coined "in-chain donor-acceptor (D-A) copolymers" based on the characteristic alternating sequence of electron-rich 'donor' and an electron-deficient 'acceptor' moieties comprising their polymer backbone. The alternating D/A moieties give rise to frontier orbitals which are, in large part, localized about the donor (for HOMO) and acceptor (for LUMO) moieties.[7] Because of this localization, the HOMO and LUMO levels can be tuned separately to achieve the optimal band gap for the semiconducting polymers. Electron density which is displaced from that of the stationary ground electronic state upon excitation to low-lying valence states is attracted by acceptor groups, and repelled by donor groups (hence the use of the term 'push/pull chromophores' in the literature to describe polymers of this design.) This effect has been shown to cause the polarization of excitons, or coulombically bound electron-hole pairs, in these materials to form partially charge-separated states henceforth referred to as 'pseudo charge-separated' (PCS) states.[8]

Until recently, the general consensus of the literature was that because complete, irreversible charge separation occurs only at phase boundaries (i.e. 'bulk heterojunction') of the donor polymer and acceptor materials,[9] whether or not excitons diffuse intact through the donor polymer or as partially separated charge carriers is of little consequence to device performance. Recent theoretical [10] and experimental [11,12] investigations of these materials are challenging this position by providing compelling evidence for both the prevalence of intramolecular charge separated states in photoexcited D-A copolymers and a strong correlation between their occurrence and the performance of resulting BHJ devices.[8] The formation of intramolecular charge-separated states in both solution-

[a] *Department of Chemistry, University of Washington, Seattle, Washington, USA. Fax: 001 206 685 8665; Tel: 001 206 685 1804; E-mail: li@chem.washington.edu.*
[b] *Dipartimento di Scienze Chimiche, Università di Napoli 'Federico II',Complesso Universitario di M.S.Angelo, via Cintia, I-80126 Napoli, Italy.*
[c] *Italian Institute of Technology, IIT@CRIB Center for Advanced Biomaterials for Healthcare, Largo Barsanti e Matteucci, I-80125 Napoli, Italy.*

phase and thin film preparations of D-A copolymers has been observed by transient absorption spectroscopy in the absence of acceptor materials.[13] Furthermore, the generation of photocurrent in neat films of these donor-acceptor block copolymers has also been experimentally verified.[12,13] Our interest in these states is two-fold. Aside from the fact that the formation of intramolecular charge-seperated states is now suspected to be linked to the performance of assembled devices[13,14] (and is therefore a process to be optimized in the design of OPV materials), the natural occurrence of charge separated states in D-A copolymer donor materials upon direct photoexcitation makes possible the theoretical investigation of individual charge carrier mobilities without requiring the application of external fields to artificially drive exciton splitting.

Beyond the advantages outlined above, the multifused-ring conjugated polymers are, in general, attractive for their superior optical and electrical properties.[15] The fused polycyclic aromatic/heteroaromatic monomers enhance the effective conjugation of the polymer backbone to facilitate electron delocalization.[16,17] Moreover, the covalently rigidified adjacent units prevent rotational disorder which reduces reorganization energy and results in a further enhancement of charge mobilities.[18,19]

Several fused-ring ladder type donor systems have been developed based on the modification of thiophene-phenylene-thiophene (also called indacenodithiophene (IDT)) skeleton, including the renowned PTB7 developed in the group of Yu.[20] In this study, we investigate three derivatives of another ladder-type D-A copolymer, poly-[(indacenodithioeno[3,2-b] thiophene)-alt-difluorobenzothiadiazole] (PIDTT-DFBT), developed by Jen et.al. which consistently yield PCEs in excess of of 7%, open-circuit voltages of 1 V, and photocurrents of 12.2 mA cm^{-2} in assembled devices.[21,22] These three derivitized polymers differ only in the composition of their donor units, which incorporate additional thiophene (T) and alkylthieno[3,2-b] thiophene (TT) into PIDTT-DFBT between D/A moieties (see Fig. 1). These modifications have been shown experimentally to improve the optical properties, solution processability, and overall performance of PIDTT-DFBT.[21] This result is somewhat counterintuitive, considering the degree of planarity of the polymer backbone (and therefore the extent of the π-conjugation/orbital delocalization) is decreased in the equilibrium nuclear geometry upon the inclusion of the T and TT groups into PIDTT-DFBT.[21] The backbone torsion permitted by the single bonds between D/A groups has been shown to result in faster charge recombination relative to completely fused ring system polymers, due to the charge carrier localization/trapping brought about by this twisting.[33]

One goal of this investigation is to identify the influence of including these T and TT groups into the polymer backbone on the mechanism and efficiency of charge transport in

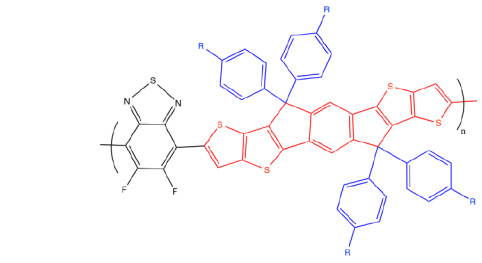

PIDTT-DFBT

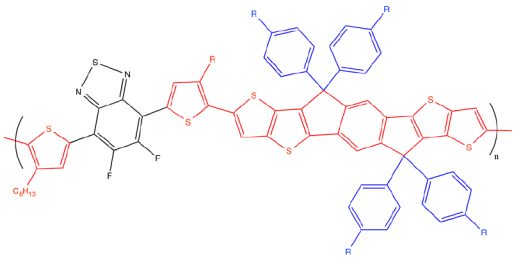

PIDTT-DFBT-T

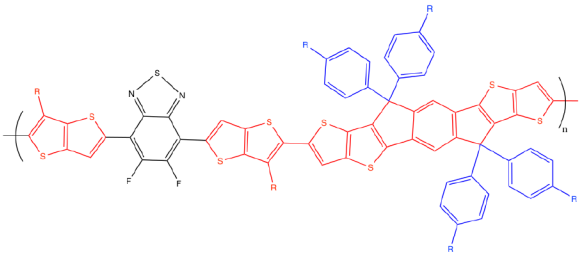

PIDTT-DFBT-TT

Fig. 1 Dimer structures for the three materials tested in the study. For the time-dependent atomic charge analysis, atoms shown in red are considered members of donor groups (D), black members of acceptor groups (A), and blue atoms' charges are neglected in this analysis as they're essentially constant in time.

these polymers. DeLongchamp et al. have recently reported that charge transport in amorphous ladder type polymer films occurs primarily along the polymer backbone, with minimal intermolecular charge-hopping mediated by π-stacking of the donor backbones.[23] To the authors' best knowledge, though, there has been no systematic study of how molecular parameters can influence these macromolecules' ability to transport charge or the orbital pathways traversed by the diffusing charge carriers following the initial excitation.

Investigations of this type lend themselves to the use of time-dependent electronic structure theories to model the evolution of excited electronic states from first principles. Real-time, time-dependent density functional theory (RT-TDDFT) is a non-perturbative approach to mean-field quantum elec-

tronic dynamics that has proven useful in this capacity, providing a better understanding of the interplay between initial photoexcited states, exciton formation, and exciton splitting to form charge-seperated states.[24,25] As such, we herein perform electronic dynamics in this formalism to explicitly track the evolution of the electronic system following excitation to the lowest-lying optically bright valence states to elucidate mechanisms of electron and hole transport in these materials. From the orbital pathways implicated in the dynamics, *p* and *n* type conductivity mechanisms may be distinguished.

2 Methodology

2.1 Many-Electron Dynamics using Real-Time Time-Dependent Density Functional Theory

The RT–TDDFT approach to many-electron dynamics is a mature method that has been applied in various computational studies of excited state dynamics, so we refer readers to our previous publications,[26,27] and only present a brief summary of the method herein.

The time evolution of a specified initial condition is resolved through RT–TDDFT calculations, in which the electronic density matrix is propagated according to the TDDFT equation in atomic units:

$$i\frac{d\mathbf{P}(t)}{dt} = [\mathbf{K}(t), \mathbf{P}(t)] \tag{1}$$

where **P** and **K** are density and Kohn-Sham matrices in an orthonormal basis. 1 is numerically integrated with a modified midpoint unitary transformation (MMUT) algorithm[26–28], where the density matrix is propagated using a unitary time evolution operator $\mathbf{U}(t_n)$:

$$\mathbf{P}(t_{n+1}) = \mathbf{U}(t_n) \cdot \mathbf{P}(t_{n-1}) \cdot \mathbf{U}^{\dagger}(t_n) \tag{2}$$

where $\mathbf{U}(t_n)$ is constructed from the eigenvectors $\mathbf{C}(t_n)$ and eigenvalues $\varepsilon(t_n)$ of the Kohn-Sham matrix at time t_n:

$$\begin{aligned}\mathbf{U}(t_n) &= \exp\left[-i \cdot 2\Delta t \cdot \mathbf{K}(t_n)\right] \\ &= \mathbf{C}(t_n) \cdot \exp\left[-i \cdot 2\Delta t \cdot \varepsilon(t_n)\right] \cdot \mathbf{C}^{\dagger}(t_n)\end{aligned} \tag{3}$$

with Δt denoting the time step.

Because the propagated single-determinantial electronic wavefunction is a coherent superposition of the relevant many-body states of the system like that observed in the instants following photon absorption, our dynamics are representative of the motion of a localized wave packet in a symplectic electronic parameter ('phase') space.[29] Wave functions of this type are the most classical, in the sense that they represent the minimum/balanced-uncertainty electronic states.[30,31] The time evolution of a fermionic state represented by a single Slater determinant can equivalently be viewed as an initially-specified point on the Grassman manifold defined by the electronic parameter space diffusing according to the TDDFT equation of motion. For readers with a background in quantum information processing, it might be beneficial to note that this Grassmannian generalizes the familiar concept of the Bloch sphere for two-state systems (i.e. qubits) to the higher dimensional, many-state case.[32]

2.2 Initial Condition and Analysis

We are interested, most generally, in the time-evolution of electronic degrees of freedom in D-A copolymer BHJ donor materials upon vertical excitation to low-lying optically-accessible excited states. The influence of incorporating additional π-bridges between the donor and acceptor units on the charge carrier dynamics is also central to this investigation. Our computational protocol is based on the following steps. First, the excited state of interest is prepared by promoting an electron from a selected occupied molecular orbital to one that is unoccupied in the ground state determinant ('Koopman excitation') according to the $S_0 \rightarrow S_1$ transition resolved by a preliminary LR-TDDFT calculation. These calculations give the $S_0 \rightarrow S_1$ transition as a nearly-pure HOMO→LUMO excitation, with no other single particle-hole transition amplitude exceeding 1%. This step creates a non-stationary electron density that is representative of a coherent superposition of the ground and excited states of interest. The coherent state is created at the ground state equilibrium nuclear geometry, simulating a vertical (Franck-Condon) photoexcitation. This state is propagated in time by numerically integrating the electronic equation of motion using Eqs. (1) to (3). In this work, we focus exclusively on the ultrafast dynamics (< 60 fs). In this time regime, the electronic dynamics are largely unaffected by the nuclear motion as observed in our previous work.[25] We expect this to be an especially suitable method for the systems investigated here owing to the extreme rigidity (i.e. large force constants) of the fused polycyclic aromatic/heteroaromatic scaffold comprising the polymer backbone.

The indiacenodithieno[3,2-b]thienophene-based polymers are modeled in this study by their minimal oligomers, i.e. as dimers. This approximation achieves a good compromise between the computational cost and accuracy of the electronic dynamics. The dimer is the smallest model for which the possibility of investigating conjugation and long-range effects along the polymer chain is preserved. For additional computational savings, the dimers have been modeled by replacing the hexyl residues along the conjugated backbone with methyl groups. We, again, refer to the findings of DeLongchamp et. al. in support of this approximation. As the polymer backbone has been implicated as the primary conduit for charge carrier

transport, we expect the truncation of these hexyl groups to minimally impact the quality of the dynamics.

In order to characterize the prepared electronic states as they evolve in time, the electron density (propagated in an orthonormal basis) is transformed into the atomic orbital (AO) basis by the Löwdin scheme. The time-dependent electron density in this basis, $\mathbf{P}'(t)$, is projected into the ground state molecular orbital space for the purpose of analysis,

$$n_i(t) = \mathbf{C'}_i^{\dagger}(0)\mathbf{P}'(t)\mathbf{C'}_i(0) \quad (4)$$

where n_i is the effective occupation number of the ground state orbital $\mathbf{C'}_i(0)$ in the AO basis.

The time-dependent dipole moment $\mu(t)$ is also calculated at each time step according to

$$\mu(t) = \mathrm{Tr}\left[\mathbf{D}'\mathbf{P}'(t)\right] \quad (5)$$

A 2.0 attosecond time step was used when integrating the TDDFT equation of motion. The molecular dipole moment was evaluated on-the-fly using 5 and natural population analysis (NPA) for atomic charges[34] was performed at 20 attosecond intervals. To simplify the presentation of the atomic charge's time evolution, the charges of all atoms comprising a given D/A moiety were summed according to definitions of acceptor and donor units outlined in Fig. 1. Cross correlation functions of the summed atomic charges of D/A subunits (see Fig. 1 for partitioning scheme) between A1-A2 and D1-D2 units were also evaluated to characterize the charge carrier separation and diffusion in these polymers according the following equation:

$$\int_{t_0}^{t_{max}} f(t)g(t+\tau)dt \quad (6)$$

In the current work, f and g are time-ordered series of summed atomic charges on moieties rather than continuous functions of time, so the integral is replaced by the discrete summation of $f \cdot g$ at different offset times τ. The t_0 occurs 10 fs into the simulation so that the analysis is representative of the charge oscillations that occur following the initial coherent recombination process. All cross-correlation function were normalized at t_0 .

All calculations were performed using a modified development version of the GAUSSIAN series of programs[35] with the addition of the MMUT–TDDFT algorithm. The hybrid PBE0 DFT functional[36–38] was used to perform both linear-response (LR) and real-time (RT) TDDFT calculations. The hybrid functionals include a fixed percentage of HF exchange (25% for PBE0). Range-corrected and range-separated hybrid functionals employ a different treatment of exchange-correlation that can potentially improve the description of charge-transfer states resolved by LR-TDDFT, but it is unclear whether the advantages of their spatially inhomogenous treatment of the exchange energy will faithfully translate from frequency-domain response type calculations to the real-time propagation. Due to the comparative nature of the current study, the potential inaccuracy of hybrid DFT exchange-correlation functionals to reproduce long-range charge transfer excitation energies is not a major concern here.

The number of basis functions per atom was minimized by employing the Stuttgart/Dresden electron-core pseudo-potentials[39] for all core electrons and the Dunning/Huzinaga full double zeta basis set[40] for the valence. The reliability of Stuttgart/Dresden pseudo-potential has been ensured by comparing the LR-TDDFT excitation energies and oscillator strengths calculated to corresponding all electron 6-31g(d) basis results (see Tab. 1).

3 Results and Discussion

	PBE0/6-31g(d)	PBE0/Stuttgart
PIDTT-DFBT	1.774 (2.12)	1.736 (1.99)
PIDTT-DFBT-T	1.727 (2.24)	1.672 (1.98)
PIDTT-DFBT-TT	1.758 (2.57)	1.715 (2.24)

Table 1 LR-TDDFT excitation energies (eV) for the $S_0 \rightarrow S_1$ transitions in the studied dimers. The corresponding oscillator strengths are reported in parenthesis.

The time-evolution of electron-hole pairs represented as time-dependent orbital occupation numbers in PIDTT-DFBT and its π-bridged analogues, computed using Eq. (4), are plotted in Fig. 2. Only orbitals at the 'band-edges' of the studied organic semiconductors exhibit large changes in their occupation, the most significant of which are plotted in Figs. 3 to 5. The frontier orbitals for each of the studied systems show similar characteristics. The HOMO band edges were found in all cases to consist of delocalized π bonding orbitals along the donor backbone, while the LUMO and LUMO+1 are (as expected) localized around acceptor moieties. Note that the LUMO is localized most heavily around A1 for each of the studied polymers with a smaller component localized around A2, and *vice versa* for the LUMO+1. LR-TDDFT calculations show that the S_1 states of these systems are dominated by the HOMO-LUMO transition. It follows then that the S_1 states are of significant charge-transfer character.

Figure 2 shows an ultrafast (< 5 fs) coherent charge transfer phenomenon after the excitation. A nearly complete recovery of the ground state is observed in the molecular orbital occupations, resulting from the attraction of the electron and hole densities of the photoexcited state. About 10 fs after photoexcitation, the electron-hole pair is still tightly bound in a coherent exciton. As the many-electron dynamics evolve, the 'push-pull' electronic gradient along the polymer backbone serves to

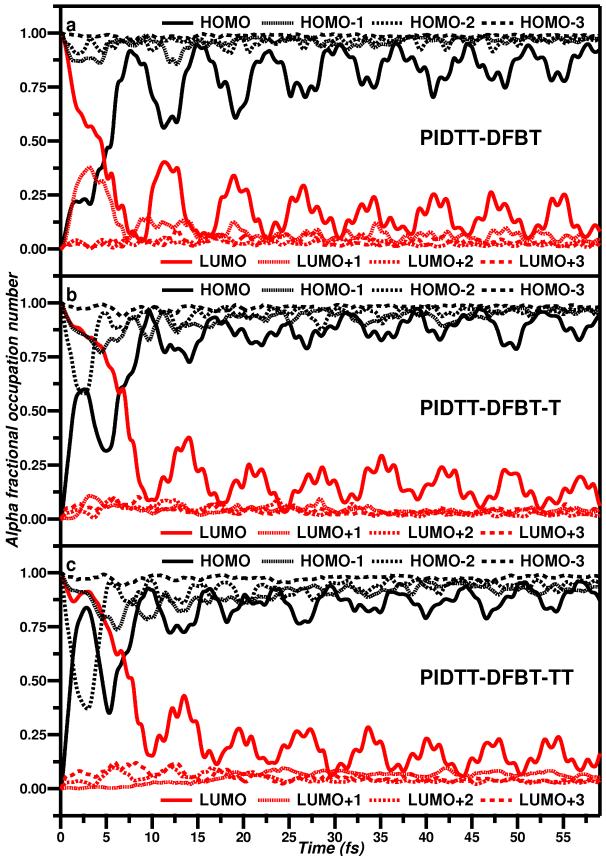

Fig. 2 Time evolving effective occupation numbers of the canonical KS orbitals (PIDTT-DFBT panel a, PIDTT-DFBT-T panel b, PIDTT-DFBT-TT panel c).

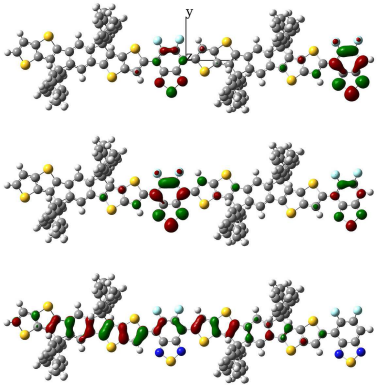

Fig. 3 Kohn-Sham orbitals (0.03 iso-density value) of PIDTT-DFBT most relevant to the density evolution evaluated at the equilibrium nuclear geometry with Cartesian axes/origin defined: LUMO+1 (upper), LUMO (mid), HOMO (lower).

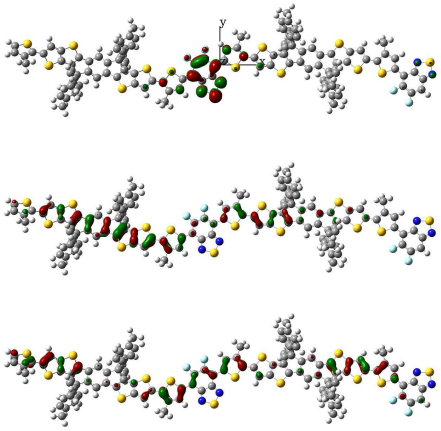

Fig. 4 Kohn-Sham orbitals (0.03 iso-density value) of PIDTT-DFBT-T most relevant to the density evolution evaluated at the equilibrium nuclear geometry with Cartesian axes/origin defined: LUMO (upper), HOMO (mid), HOMO-2 (lower).

quickly polarize this exciton, leading to the charge-separated state indicated by the long-lived, correlated oscillations in the HOMO and LUMO contributions to the time-evolving electron density.

While all three of the dimers share similar timescales for the formation and partial separation of the exciton following photo-excitation to the S_1 state, the orbital pathways by which these states evolve in the earliest femtoseconds following excitation differ drastically. In polymers containing additional π-bridges between groups, an ultrafast loss of HOMO occupation and correlated rise in HOMO-2 occupation is observed. A similar correlation in the unoccupied manifold between the LUMO and LUMO+1 occupations occurs for PIDTT-DFBT. This discrepancy suggests different mechanisms for the formation of excitons from the photoexcited valence states in PIDTT-DFBT and its π-bridged analogues. For PIDTT-DFBT, occupation fluctuates between LUMO (localized heavily around A1) and LUMO+1 (localized about A2), indicating the translation of electron density along the polymer to form the exciton. However, it is the holes in PIDTT-DFBT-T and PIDTT-DFBT-TT which relax to lower energy

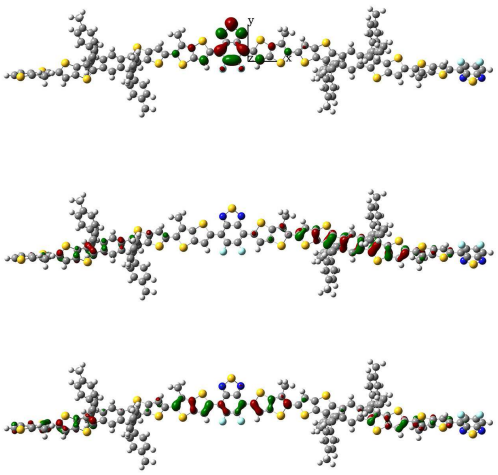

Fig. 5 Kohn-Sham orbitals (0.03 iso-density value) of PIDTT-DFBT-TT most relevant to the density evolution evaluated at the equilibrium nuclear geometry with Cartesian axes/origin defined: LUMO (upper), HOMO (mid), HOMO-2 (lower).

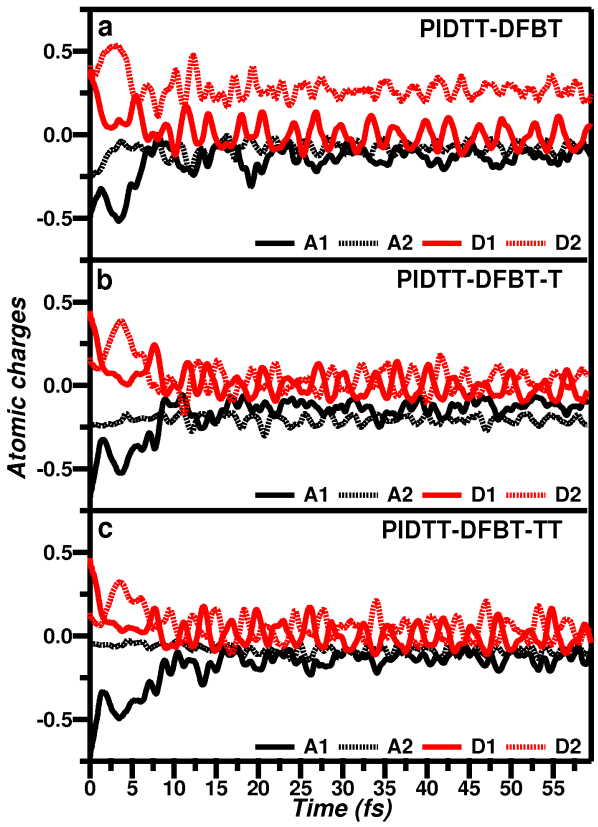

Fig. 6 Summed NPA charges for Donor and Acceptor blocks 1 and 2: (a) PIDTT-DFBT, (b) PIDTT-DFBT-T, and (c) PIDTT-DFBT-TT.

orbitals in the occupied manifold, suggesting hole migration as the short-time charge migration mechanism that mediates exciton formation in these systems. This result is lent credence by experimental evidence that electron mobilities are orders of magnitude greater in PIDTT-DFBT than its T or TT analogues as measured in gated field-effect organic transistor experiments.[21] Experimental investigations of hole mobility are also consistent with out results, showing increasing hole mobility as larger π bridges are introduced between D/A groups.[41]

The electronic dynamics in the 10–50 fs regime show long-lived charge oscillations that follow the S_1 state's ultrafast internal conversion to the excitonic state. Memory of the electron and hole kinetic energies prior to exciton formation are encoded into the latent charge oscillations. In order to better understand the spatial diffusion characteristics of the electron and hole densities, time evolving atomic charges were computed and summed over D/A moieties. The evolution of these summed moiety charges are given in Fig. 6. Within the first $\sim$5 fs, the large degree of charge separation associated with the initial photoexcited charge-transfer state starts to decay, indicating the formation of the bound exciton. At $\sim$10 fs, the bound exciton succumbs to the polymer's push-pull nature and partially dissociates, yielding the charge-separated states indicated by the out-of-phase (anti-correlated) oscillation of charge along the polymer. These oscillations would persist indefinitely, as our calculations allow no coupling to phonon modes or the environment to provide a means to decohere the electronic state and dissipate the extra energy associated with the initial excitation. Because the nuclear geometry is fixed throughout the electronic propagation, differences in the dynamics of the three systems are strictly the result of changes in the transition moments between electronic states that are induced by the incorporation of the additional π-spacers. However, since the inclusion of T and TT groups affects the degree of planarity of these system's equilibrium geometries, we have also indirectly probed the effect of backbone planarity on the charge carrier diffusion.

From inspection, the summed charges on the first and second donor groups (D1/D2) and on the first donor and acceptor (A1/D1) both appear to be correlated. The A1/D1 correlation in the earliest 10 fs is an artifact of the coherent recombination of the photoexcited CT state to form the exciton. D1/D2 and

A1/A2 correlations in the 10–50 fs range can be attributed to hole and electron transport respectively. To better quantify the relationships between the oscillation of charge between groups in these systems, cross correlation functions were calculated between the time-evolving D1/D2 and A1/A2 charges (see Fig. 7.)

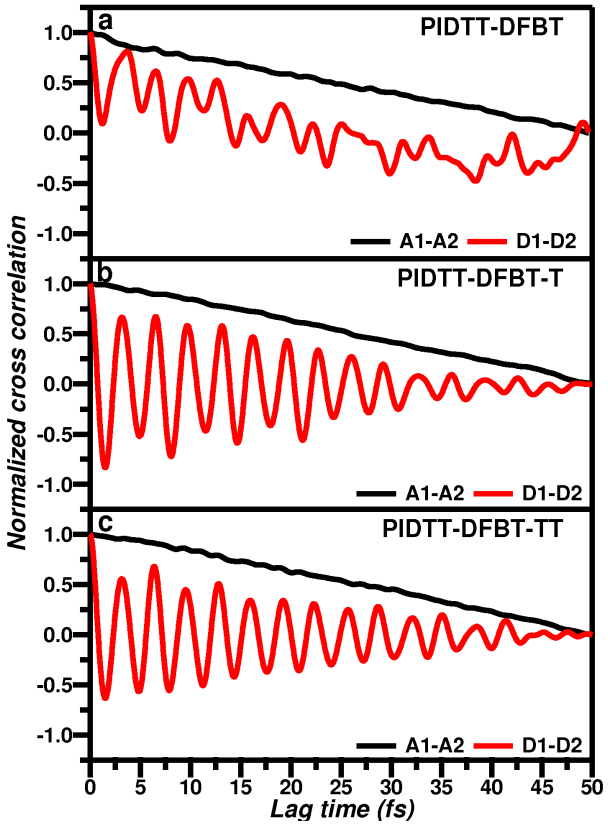

Fig. 7 Cross-correlation functions between D1/ D2 charges and A1/ A2 charges indicative of hole and electron diffusion along the polymer backbone respectively (PIDTT-DFBT panel a, PIDTT-DFBT-T panel b, PIDTT-DFBT-TT panel c).

Minima in these cross correlation functions occur for offset times that result in the charge oscillations on the relevant groups being out-of-phase with one another whereas maxima in the cross-correlation function signify offset times that yield a maximum coincidence of the two time-ordered series. Only the oscillation of separated charge-carriers (not the migration of an intact exciton) will give rise to the loss of charge density on one moiety and simultaneous rise in charge density on another displayed in Fig. 7, as the bound electron-hole pair is a net neutral quasiparticle that would not significantly change the summed charge of a D/A unit upon passage to/from that unit. A cross-correlation function corresponding to the separated charge carrier motion would show oscillatory behavior with a frequency defined by the rate of the charge oscillations. The frequencies of these oscillations are one measure of the charge carrier mobilities in these dimers, with the constant of proportionality given by the distance separating the groups hosting the charge oscillations. Fourier analysis was carried out for each of the cross correlation functions (Fig. 8), exposing the frequencies contributing to the complicated charge dynamics.

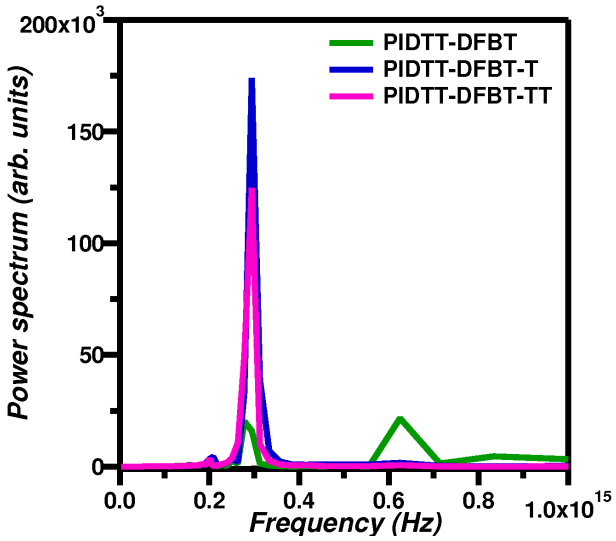

Fig. 8 Fourier transform mod squared (i.e. 'power spectrum') of the D1/D2 charge cross-correlation functions indicating hole mobilities in the studied systems (PIDTT-DFBT green, PIDTT-DFBT-T blue, PIDTT-DFBT-TT magenta).

Even though the principle oscillatory frequencies of charges in the studied systems are largely unaffected by the addition of the T or TT groups, the distance between D/A groups is increased by the addition of these groups. The inclusion of the spacer apparently has a vanishingly small effect on the transition moments between the relevant electronic states, but the states themselves are more spatially diffuse, resulting in the heightened charge carrier mobility observed in the T and TT derivatives. This important result provides qualitative insight into our primary question of how the inclusion of π spacers between the D/A blocks of PIDTT affects charge mobilities in these materials. Excitation to the S_1 state in these polymers results in charge carrier velocities which are roughly proportionate to the extra backbone length afforded by the T or TT groups relative to PIDTT-DFBT.

Without the ability to individually resolve the electron and hole contributions to the charge dynamics, this frequency analysis is ultimately unable to fully explain the charge carrier mobility in these systems. Without this level of detail, the

origins of the higher-frequency contributions to the PIDTT-DFBT power spectrum are also unclear.

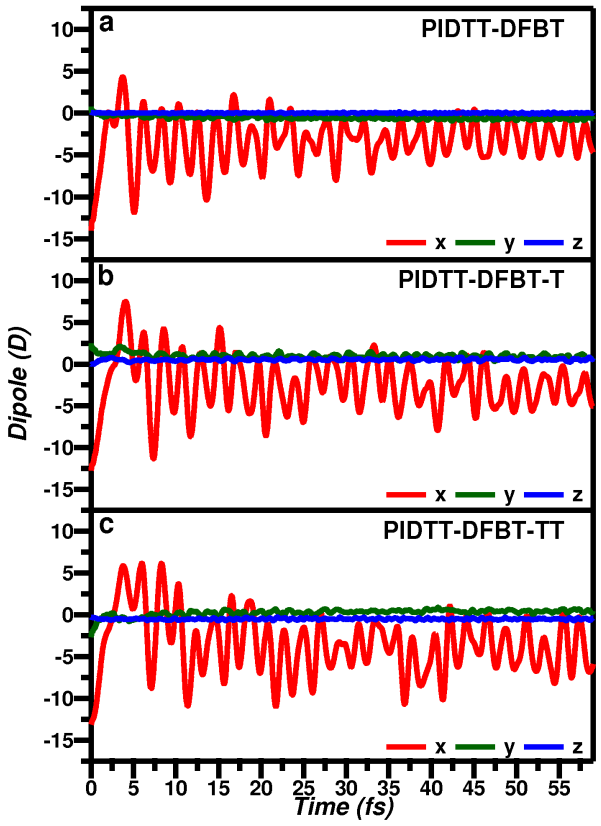

Fig. 9 Time-evolving electric dipole along each Cartesian axis (see Fig. 3 for coordinate definitions)

The oscillation of charge between spatially separated moieties naturally gives rise to a dynamic electric dipole moment. This electric dipole moment was calculated during the electronic dynamics, and its individual Cartesian components are plotted in Fig. 9. The large-amplitude oscillations in the 5 fs range occur at the onset of exciton formation, and the transition to lower amplitude oscillations which persist for the duration of the simulation at ∼10 fs coincides with the onset of charge separation. While the electric dipole analysis does at least provide the magnitude and direction of charge separation that our frequency analysis lacks, a complete depiction of the charge transport process requires absolute spatial resolution for the electron and hole densities. Accordingly, we have calculated the barycenters of the electron ($\bar{\mathbf{R}}_e$) and hole ($\bar{\mathbf{R}}_h$) densities from the NPA charges according to Eqs. (7) to (9), where $A(-)$ and $A(+)$ are indices for atoms with NPA charge differences, $\tilde{q}_A$, that are negative and positive respectively. Atomic charge differences are calculated by subtracting the ground state charge, $q_A(0)$, from the instantaneous charge.

$$\tilde{q}_A(t) = q_A(t) - q_A(0) \tag{7}$$

$$\bar{\mathbf{R}}_e(t) = \Big(\sum_{A(-)} \tilde{q}_{A(-)}\Big)^{-1} \sum_{A(-)} \tilde{q}_{A(-)}\mathbf{R}_{A(-)} \tag{8}$$

$$\bar{\mathbf{R}}_h(t) = \Big(\sum_{A(+)} \tilde{q}_{A(+)}\Big)^{-1} \sum_{A(+)} \tilde{q}_{A(+)}\mathbf{R}_{A(+)} \tag{9}$$

The application of this analysis finally reveals the pseudo-classical picture for the translation of these charge distributions along the polymer chain that was only alluded to in the oscillations of the moiety's summed atomic charges. The initial attraction experienced by the electron and hole densities, ultra-short lifetime for the tightly-bound exciton, and the separation of the positive and negative charge densities are exposed explicitly, as seen in Fig. 10. With this spatially-resolved analysis, we can also identify recurrences of the tightly-bound excitonic state following the initial polarization of the exciton, where the separated electron and hole densities collide and drag one another along a mutual trajectory for a few oscillatory periods before reseparating.

With the time evolution of the first moment of the electron and hole distributions in place, we can directly evaluate the average velocities of these pseudo particles for each of the dimers. $\bar{\mathbf{R}}_e$ and $\bar{\mathbf{R}}_h$ were numerically differentiated by the central difference algorithm, and the resulting velocities were averaged over the first 50 fs of the dynamics. The RMS electron and hole barycenter velocities are given in Tab. 2, and are consistent with our previous analysis of the frequency of charge oscillations along the dimers as well as the experimental trends mentioned above. Recall, though, that these free charge-carrier velocities are affected by both the choice of DFT functional and the deviations of the initial electronic state from the true S_1 state. So, while these results can be cautiously interpreted to establish a qualitative trend in the carrier velocities, their absolute accuracy cannot be guaranteed.

	$\dot{\bar{\mathbf{R}}}_e$	$\dot{\bar{\mathbf{R}}}_h$
PIDTT-DFBT	0.01314	0.01373
PIDTT-DFBT-T	0.01464	0.01525
PIDTT-DFBT-TT	0.01482	0.01557

Table 2 RMS electron and hole barycenter velocities in Å/attosecond.

It is ultimately not clear from the results for the simple dimers whether long-range charge transport along the backbone of realistically-sized polymers can be correctly simulated by such a minimal model, especially considering the charge carrier mobility has been shown experimentally to correlate

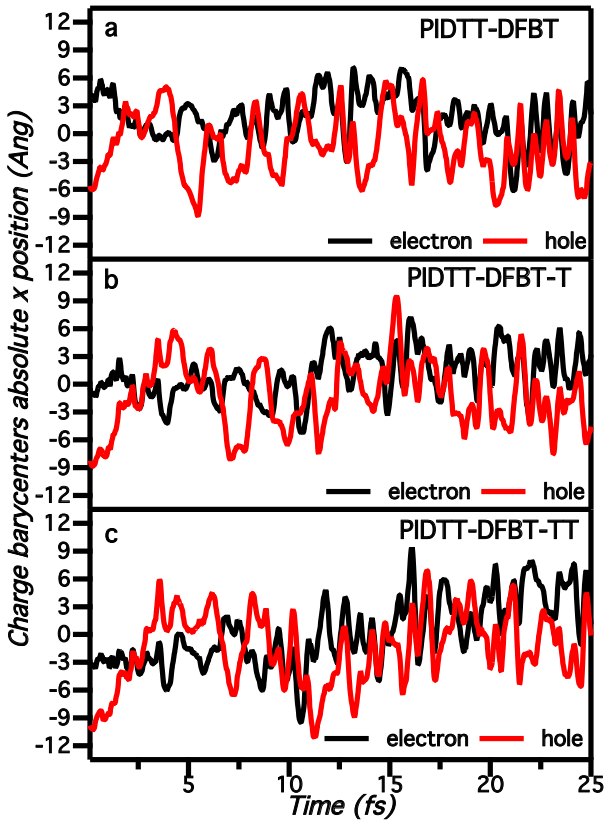

Fig. 10 Time-evolution of the electron and hole barycenter positions along the *x* axis in the studied systems. (see Fig. 3 for coordinate definitions)

with the length of the polymer chain.[23] However, we have shown that the average separation of the electron and hole barycenters upon excitation to the S_1 state of the dimers is at all times much less than the length of the dimers themselves, suggesting that our model is sufficiently large to be outside of the strongly quantum confined regime. However, it does not follow that the electronic dynamics of the dimer are entirely representative of those for polymers of realistic molecular weights. Specifically, the tails of the electron and hole densities do migrate out to the ends of the dimer during the dynamics, and respond by reflecting off the ends as if scattering from an infinitely high potential barrier.

One might also question whether photoexcited states in which the electron and hole densities are initially further separated along the polymer chain would give rise to charge carriers of even greater velocities due to the longer duration that the electron and hole densities may be mutually accelerated towards one another through their Coulomb interaction. While these states might yield 'hotter' charge-carriers, they are of limited relevance since the oscillator strengths for transitions to a state diminish quadratically with the spatial overlap of the particle and hole wave functions. So, while states of significantly greater charge separation may exist, they quickly become dipole disallowed transitions from the ground state and thus we can be confident that states with electron and hole wave functions localized to adjacent D/A groups like the S_1 states modeled herein are the most physically relevant regardless of polymer length. This line of reasoning brings to light a troubling dilemma for the design of new semiconducting organic chromophores for OPV devices. Ideal OPV materials must balance the need for a strongly allowed optical absorption to maintain high external quantum efficiency with the need for a high degree of charge separation in the photoexcited state to generate high-velocity charge carriers that support high internal quantum efficiency; two properties which are fundamentally at odds with one another. This argument disregards the occurrence of inter-chain excitations (i.e. electron on one chain, hole on another), which are infrequent even in the disordered bulk of assembled BHJ devices and therefore exert little influence on the overall device performance.[12]

4 Conclusion

In this work, we have applied mean-field, non-perturbative electronic dynamics in the TDDFT formalism to resolve, in real time, the dynamics of charge carriers in ladder-type donor-acceptor block copolymers. Coherent, excited states representative of slightly perturbed S_1 states of these systems were prepared and propagated in time, resulting in electronic dynamics that in all cases showed signatures of charge transfer, exciton formation, and long-lived charge oscillation between donor and acceptor groups attributed to the pseudo charge-separated state. Within 5 fs of photo-excitation, the electron and hole densities attract one another and partially recombine to form a tightly-bound exciton. The orbital pathways involved in these short-time dynamics suggest a predominantly n-type conduction mechanism to be in effect for PIDTT-DFBT and p-type for its π-spaced analogues. Shortly after the formation of the exciton, the electron and hole densities are strongly influenced by the electronic gradient along the polymer and partially dissociate to yield a pseudo charge-separated state, with short-lived revivals of the exciton occasionally resulting from collisions between the separated electron and hole densities.

5 Acknowledgement

Financial support from the US National Science Foundation (CHE-1265945), the Department of Energy (DE-SC0006863), and additional support from the University of Washington Stu-

dent Technology and Royalty Research Fund are gratefully acknowledged.

References

1 J. Chen and Y. Ca, *Acc. Chem. Res.*, 2009, **42**, 1709–1718.
2 Y.-J. Cheng, S.-H. Yang and C.-S. Hsu, *Chem. Rev.*, 2009, **109**, 5868–5923.
3 Z. He, C. Zhong, X. Huang, W.-Y. Wong, H. Wu, L. Chen, S. Su and Y. Cao, *Adv. Mater.*, 2011, **23**, 4636–4643.
4 T. Yang, M. Wang, C. Duan, X. Hu, L. Huang, J. Peng, F. Huang and X. Gong, *Energ. Environ. Sci.*, 2012, **5**, 8208–8214.
5 Y. Zhang, J. Zou, C.-C. Cheuh, H.-L. Yip and A. K.-Y. Jen, *Macromolecules*, 2012, **45**, 5427–5435.
6 C. Duan, F. Huang and Y. Cao, *J. Mater. Chem.*, 2012, **22**, 10416–10434.
7 J. Nelson, *Mater. Today*, 2011, **14**, 462 – 470.
8 B. S. Rolczynski, J. M. Szarko, H. J. Son, Y. Liang, L. Yu and L. X. Chen, *J. Am. Chem. Soc.*, 2012, **134**, 4142–4152.
9 A. Petersen, A. Ojala, T. Kirchartz, T. A. Wagner, F. Würthner and U. Rau, *Phys. Rev. B*, 2012, **85**, 245208–245218.
10 D. Caruso and A. Troisi, *Proc. Natl. Acad. Sci. U.S.A.*, 2012, **109**, 13498–13502.
11 S. Glinas, A. Rao, A. Kumar, S. L. Smith, A. W. Chin, J. Clark, T. S. van der Poll, G. C. Bazan and R. H. Friend, *Science*, 2014, **343**, 512–516.
12 O. G. Reid, R. D. Pensack, Y. Song, G. D. Scholes and G. Rumbles, *Chem. Mater.*, 2014, **26**, 561–575.
13 J. M. Szarko, B. S. Rolczynski, S. J. Lou, T. Xu, J. Strzalka, T. J. Marks, L. Yu and L. X. Chen, *Adv. Func. Mater.*, 2014, **24**, 10–26.
14 B. Carsten, J. M. Szarko, H. J. Son, W. Wang, L. Lu, F. He, B. S. Rolczynski, S. J. Lou, L. X. Chen and L. Yu, *J. Am. Chem. Soc.*, 2011, **133**, 20468–20475.
15 Z.-G. Zhang and J. Wang, *J. Mater. Chem.*, 2012, **22**, 4178–4187.
16 Q. Zheng, B. J. Jung, J. Sun and H. E. Katz, *J. Am. Chem. Soc.*, 2010, **132**, 5394–5404.
17 J.-S. Wu, Y.-J. Cheng, M. Dubosc, C.-H. Hsieh, C.-Y. Chang and C.-S. Hsu, *Chem. Commun.*, 2010, **46**, 3259–3261.
18 C. Schwarz, H. Bässler, I. Bauer, J.-M. Koenen, E. Preis, U. Scherf and A. Köhler, *Adv. Mater.*, 2012, **24**, 922–925.
19 J. Roncali, *Macromol. Rapid Commun.*, 2007, **28**, 1761–1775.
20 Y. Liang, Z. Xu, J. Xia, S.-T. Tsai, Y. Wu, G. Li, C. Ray and L. Yu, *Adv. Mater.*, 2010, **22**, 135–138.
21 J. J. Intemann, K. Yao, Y.-X. Li, H.-L. Yip, Y.-X. Xu, P.-W. Liang, C.-C. Chueh, F.-Z. Ding, X. Yang, X. Li, Y. Chen and A. K.-Y. Jen, *Adv. Func. Mater.*, 2014, **24**, 1465–1473.
22 Y.-X. Xu, C.-C. Chueh, H.-L. Yip, F.-Z. Ding, Y.-X. Li, C.-Z. Li, X. Li, W.-C. Chen and A. K.-Y. Jen, *Adv. Mater.*, 2012, **24**, 6356–6361.
23 X. Zhang, H. Bronstein, A. J. Kronemeijer, J. Smith, Y. Kim, R. J. Kline, L. J. Richter, T. D. Anthopoulos, H. Sirringhaus, K. Song, M. Heeney, W. Zhang, I. McCulloch and D. M. DeLongchamp, *Nat. Commun.*, 2013, **4**, 2238:1–9.
24 C. T. Chapman, W. Liang and X. Li, *J. Phys. Chem. Lett.*, 2011, **2**, 1189–1192.
25 F. Ding, C. T. Chapman, W. Liang and X. Li, *J. Chem. Phys.*, 2012, **137**, 22A512.
26 X. Li, S. M. Smith, A. N. Markevitch, D. A. Romanov, R. J. Levis and H. B. Schlegel, *Phys. Chem. Chem. Phys.*, 2005, **7**, 233–239.
27 W. Liang, C. T. Chapman and X. Li, *J. Chem. Phys.*, 2011, **134**, 184102.
28 C. M. Isborn, X. Li and J. C. Tully, *J. Chem. Phys.*, 2007, **126**, 134307.
29 M. Yamamura and A. Kuriyama, *Progress of Theoretical Physics Supplement*, 1987, **93**, 1–175.
30 D. J. Rowe, A. Ryman and G. Rosensteel, *Phys. Rev. A*, 1980, **22**, 2362–2373.
31 A. Sugita, *J. Phys. A Math. Gen.*, 2003, **36**, 9081–9103.
32 E. Tirapegui and W. Zeller, *Instabilities and Nonequilibrium Structures IV*, Springer Netherlands, 1993, pp. 27–36.
33 Y. Li, K. Yao, H.-L. Yip, F. Ding, Y.-X.Xu, X. Li, Y. .Chen and A. K. Jen, *Adv. Func. Mater.*, 2014, **24**, 3631–3638.
34 A. E. Reed, R. B. Weinstock and F. Weinhold, *J. Chem. Phys.*, 1985, **83**, 735.
35 M. J. Frisch, G. W. Trucks, H. B. Schlegel, G. E. Scuseria, M. A. Robb, J. R. Cheeseman, G. Scalmani, V. Barone, B. Mennucci, G. A. Petersson, H. Nakatsuji, M. Caricato, X. Li, H. P. Hratchian, A. F. Izmaylov, J. Bloino, G. Zheng, J. L. Sonnenberg, W. Liang, M. Hada, M. Ehara, K. Toyota, R. Fukuda, J. Hasegawa, M. Ishida, T. Nakajima, Y. Honda, O. Kitao, H. Nakai, T. Vreven, J. J. A. Montgomery, J. E. Peralta, F. Ogliaro, M. Bearpark, J. J. Heyd, E. Brothers, K. N. Kudin, V. N. Staroverov, T. Keith, R. Kobayashi, J. Normand, K. Raghavachari, A. Rendell, J. C. Burant, S. S. Iyengar, J. Tomasi, M. Cossi, N. Rega, J. M. Millam, M. Klene, J. E. Knox, J. B. Cross, V. Bakken, C. Adamo, J. Jaramillo, R. Gomperts, R. E. Stratmann, O. Yazyev, A. J. Austin, R. Cammi, C. Pomelli, J. W. Ochterski, R. L. Martin, K. Morokuma, V. G. Zakrzewski, G. A. Voth, P. Salvador, J. J. Dannenberg, S. Dapprich, P. V. Parandekar, N. J. Mayhall, A. D. Daniels, O. Farkas, J. B. Foresman, J. V. Ortiz, J. Cioslowski and D. J. Fox, *Gaussian Development Version Revision H.12+*, Gaussian Inc., Wallingford CT 2011.
36 C. Adamo and V. Barone, *J. Chem. Phys.*, 1999, **110**, 6158.
37 J. P. Perdew, K. Burke and M. Ernzerhof, *Phys. Rev. Lett.*, 1996, **77**, 3865–3868.
38 J. P. Perdew, K. Burke and M. Ernzerhof, *Phys. Rev. Lett.*, 1997, **78**, 1396–1396.
39 G. Igel-Mann, H. Stoll and H. Preuss, *Mol. Phys.*, 1988, **65**, 1321–1328.
40 T. H. D. Jr and P. J. Hay, *Methods of electronic structure theory*, Springer, 1977, pp. 1–27.
41 Y.-J. Cheng, S.-W. Cheng, C.-Y. Chang, W.-S. Kao, M.-H. Liao and C.-S. Hsu, *Chem. Commun.*, 2012, **48**, 3203–3205.